

# Origin and Control of Adhesion between Emulsion Drops Stabilized by Thermally Sensitive Soft Colloidal Particles

Mathieu Destribats,<sup>\*,†,‡</sup> Véronique Lapeyre,<sup>§</sup> Elisabeth Sellier,<sup>⊥</sup> Fernando Leal-Calderon,<sup>||</sup> Valérie Ravaine,<sup>§</sup> and Véronique Schmitt<sup>\*,†</sup>

<sup>†</sup>Université Bordeaux 1, Centre de Recherche Paul Pascal, CNRS, 115 Av. A. Schweitzer, 33600 Pessac, France

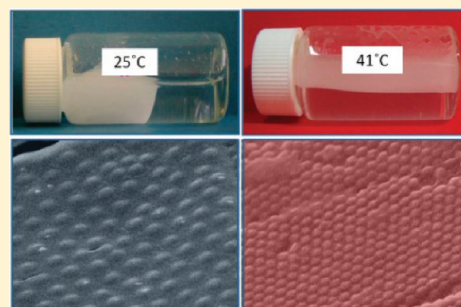
<sup>§</sup>Université Bordeaux 1, Institut des Sciences Moléculaires, ENSCBP, 16 Av. Pey Berland, 33607 Pessac Cedex, France

<sup>||</sup>Université Bordeaux 1, Laboratoire de Chimie et Biologie des Membranes et des Nano-objets, CNRS, Allée Geoffroy St Hilaire, Bât B14, 33600 Pessac, France

<sup>⊥</sup>CREMEM, Université Bordeaux 1, Bât. B8, Avenue des Facultés, 33405 Talence, France

## Supporting Information

**ABSTRACT:** We used soft microgels made of poly(*N*-isopropylacrylamide) (pNIPAM) of variable cross-linking degrees and the same colloidal size to stabilize oil-in-water Pickering emulsions. The extent of droplet flocculation increased and the resistance of the emulsions to mechanical stresses decreased as the cross-linking density was augmented. Large flat films were separating the droplets, and we could measure the adhesion angle at the junction with the free interfaces through several microscopy methods. The size of the flat films and the values of the angles were reflecting strong adhesive interactions between the interfaces as a result of microgel bridging. In parallel, cryo-SEM imaging of the thin films allowed a precise determination of their structure. The evolution of the adhesion angle and of the film structure as a function of microgels cross-linking density provided interesting insights into the impact of particle softness on film adhesiveness and emulsion stability. We exploited our main findings to propose a novel route for controlling the emulsions end-use properties (flocculation and stability). Owing to particle softness and thermal sensitivity, the interfacial coverage was a path function (it depended on the sample “history”). As a consequence, by adapting the emulsification conditions, the interfacial monolayer could be trapped in a very dense and rigid configuration, providing improved resistance to bridging flocculation and to flow-induced coalescence.



## ■ INTRODUCTION

Emulsions are metastable materials comprised of two immiscible fluids, such as oil and water, used for many industrial applications, such as cosmetics, foods, pharmaceuticals, paintings, coatings, etc. They are generally obtained in the presence of different surface-active species, such as surfactant molecules, amphiphilic polymers, or proteins.<sup>1</sup> It is now well established that solid particles of colloidal size may also be employed to kinetically stabilize emulsions. The so-called Pickering emulsions<sup>2,3</sup> or, more generally, solid-stabilized emulsions can be obtained with a wide variety of solid organic particles, mineral powders, and even naturally occurring particles.<sup>4,5</sup> Such materials have received considerable interest in recent years, not only because of their importance in a range of practical applications but also because of their uniqueness in the stabilization mechanisms in comparison to ordinary surfactants. The peculiar stabilizing properties mainly arise from the colloidal size of the particles and their irreversible anchoring at the oil–water interface.<sup>1,4,5</sup> The two main destabilizing processes that occur in emulsions are coalescence and Ostwald ripening.<sup>1</sup> In either case, the droplet surface area is reduced and surface-active materials can become compressed at

the interface. Because of their relevance in understanding the behavior of emulsions, particle monolayers at oil–water interfaces have motivated numerous studies.<sup>6–9</sup> One of the key issues is the structural understanding of phase behavior during compression. As a monolayer is compressed, it undergoes a series of phase transitions due to the reduction in area available per particle. Much attention has been given to the relationship between the structural changes and the interactions of the adsorbed particles. Repulsive particles may generate loosely packed 2D crystals, whose compression/expansion is controlled by surface tension. Upon compression of the monolayers, hexagonal arrays of nearly close-packed particles can be achieved, and in this limit, the interfaces exhibit “solid”-like behavior.<sup>10</sup> The fluid-to-solid transition is manifested in buckling or wrinkling of the interfaces.<sup>10,11</sup> In some cases, the adsorbed particles experience pronounced lateral attractive forces. For instance, rigid particles (silica, latex) may locally deform the interfaces and generate capillary interactions

**Received:** November 7, 2011

**Revised:** December 28, 2011

**Published:** January 20, 2012

whose intensity can be as large as several thousand times the thermal energy.<sup>12</sup> A close-packed monolayer of attractive particles at the air–water interface may behave as a 2D elastic solid and can support anisotropic stresses and strains: it buckles in uniaxial compression and becomes smooth again when the compressive stress is removed.<sup>13–17</sup> For strongly attractive particles, a 2D plastic behavior has been reported<sup>18</sup> and the interface does not relax its shape after cessation of an applied stress.<sup>19–21</sup>

The emulsion lifetime is mainly determined by the properties of thin liquid films that are metastable assemblies formed in between adjacent droplet interfaces. When dealing with solid-stabilized emulsions, two limiting situations can be envisioned concerning thin film structure: the particles may form a bilayer or a monolayer. In this latter case, the particles bridge the interfaces when two drops come into close proximity, forming a dense monolayer that prevents or retards the film from draining. Single model film experiments have shed light into the structural changes that occur during film thinning.<sup>9,22–24</sup> In these experiments, interfaces covered by micrometer-sized rigid particles were brought into contact in a controlled manner and their structure was followed by optical microscopy. Various scenarios leading to bridged monolayers were identified under well-controlled conditions. When the two interfaces were close enough, the particles at both interfaces arranged in such a way that the particles at one interface filled the interstices of particle lattices on the opposing interface, followed by a rapid growth of a dense particle aggregate of disk shape that resisted further coalescence between the two interfaces. The particle aggregate was found to be only one monolayer thick that spanned the two interfaces, which is consistent with a bridging configuration.<sup>9,22–24</sup> In some other cases, the particles from one of the interfaces were repelled away from the contact region and let the particles from the other interface bridge the surfaces.<sup>25</sup> Single model film experiments also demonstrated that particle monolayers produced strong adhesive forces per unit area, far more than the Laplace pressure of the drops under study.<sup>23</sup>

The design of emulsions which can evolve under the effect of an external stimulus is highly sought-after, as it is advantageous and of practical interest to destabilize emulsions “on demand”, by simply modifying one variable in the system. Soft particles such as microgels made of a cross-linked polymer that is swollen in good solvent may act as stimulus-responsive particulate emulsifiers owing to their pH<sup>26–31</sup> or thermoresponsive properties.<sup>32,33</sup> Poly(*N*-isopropylacrylamide) (pNIPAM) microgels that are well-known for their sensitivity to temperature are of special relevance within this purpose. They are swollen by water below the so-called volume phase transition temperature (VPTT = 33 °C) and shrink when heated above it.

In a recent study,<sup>34,35</sup> we probed the stability of flocculated emulsions stabilized by soft pNIPAM microgel particles whose deformability was tuned by varying their internal cross-linking density or the temperature. Contrarily to most of the studies reported in the literature, the used microgels were only thermoresponsive but not pH-responsive. We provided experimental evidence that the initially spherical microgels were flattened at the interface and adopted a “fried-egg-like” morphology due to their core–shell structure (see Supporting Information Figure S1). The most deformable microgels tended to form 2D connected networks characterized by significant overlapping of the peripheral parts (filaments or digitations). When the microgel deformability was lost, either

by increasing the cross-linking density or the temperature, the stabilization efficiency was considerably reduced. Indeed, emulsions stabilized by the more cross-linked microgels were stable during storage but very fragile and almost not handleable. Increasing the temperature above the VPTT induced an oil–water phase separation. In this previous study, the emulsion stability was discussed in light of the morphology of the microgels adsorbed on free interfaces, *i.e.* not in direct contact with neighboring drops.

The scope of the present paper is different and complementary since we carefully examined films between adjacent drops. Indeed, we investigated the impact of microgels cross-linking density on the formation of adhesive films between oil-in-water drops in order to identify the main parameters governing emulsion properties (stability against coalescence and flocculation). In real situations, the interfaces undergo dilatational stresses because of buoyancy driven phenomena and external mechanical disturbances (agitation). Although extremely useful, single thin film experiments consisting in the controlled approach of two interfaces are not necessarily addressing all the possible scenarios in terms of film formation. In the study reported here, our strategy was thus based on direct observations of real emulsion films. When emulsification was carried out at room temperature, droplets were flocculated and separated by very large flat films. By measuring the film size and the angle at the junction with the free interfaces, we estimated the adhesive interactions between the interfaces. Using cryo-SEM face and edge views of the films, we proposed a precise description of their internal structure and their evolution with the microgel cross-linking density. By gathering microscopic and macroscopic observations, it was possible to assess the impact of particle softness on film adhesiveness and emulsion stability. Owing to the acquired knowledge, we proposed a method to suppress aggregation and improve the stability under mechanical stress of the emulsions.

Besides the application field, which is considerably widespread, the thermodynamics of soft amphiphilic colloids at interfaces is an emerging field, and this manuscript aims at identifying some key differences between soft colloids and solid particles as emulsions stabilizers.

## MATERIALS AND METHODS

**1. Materials.** All the reagents were purchased from Sigma-Aldrich, unless otherwise specified. *N*-Isopropylacrylamide (NIPAM) was recrystallized from hexane (provided from ICS) and dried under vacuum prior to use. *N,N'*-Methylenebisacrylamide (BIS) and potassium persulfate (KPS) were used as received. Milli-Q water was used for all synthesis reactions, purification, solution preparation, and emulsion fabrication. Hexadecane, dodecane, and heptane (Sigma-Aldrich, purity >99%) were used without further purification.

**2. Particles Synthesis and Purification.** We synthesized pNIPAM microgels of various cross-linking densities characterized by the relative molar % of BIS segments (from 1.5 to 10 mol % introduced during the synthesis). The microgels were obtained by an aqueous free-radical precipitation polymerization classically employed for the synthesis of thermoresponsive microgels and especially pNIPAM microgels.<sup>34,36</sup> Polymerization was performed in a 500 mL three-neck round-bottom flask, equipped with a magnetic stir bar, a reflux condenser, a thermometer, and an argon inlet. The initial total monomer concentration was held constant at 62 mM. NIPAM and BIS were dissolved in 98 mL of water. The solutions were purified through a 0.2  $\mu$ m membrane filter to remove residual particulate matter. The solutions were then heated up to 70 °C with argon thoroughly bubbling during at least 1 h prior to initiation. Free radical polymerization was then initiated with KPS (2.5 mM) dissolved in 2

mL of water. The initially transparent solutions became progressively turbid as a consequence of the polymerization process. The solutions were allowed to react for a period of 6 h in the presence of argon under stirring. The microgels were purified by centrifugation–redispersion cycles at least five times (21 000g for 1 h, where  $g$  is the gravity constant). For each cycle, the supernatant was removed and its surface tension was measured by the pendant drop method. The purification was repeated until the surface tension of the supernatant reached that of pure water, *i.e.* above 70 mN·m<sup>−1</sup>.

**3. Particles Dispersion Characterization.** Particles size and polydispersity were determined by photon correlation spectroscopy (PCS) at a detection angle of 90°, using a ZetasizerNano S90 Malvern Instrument equipped with a HeNe laser. The hydrodynamic diameters were calculated from diffusion coefficients using the Stokes–Einstein equation. All analyses were performed with the software supplied by the manufacturer. The polydispersity index (PDI) was derived from the cumulant analysis method.

The polymer content  $c_{\text{polymer}}$  (in g·cm<sup>−3</sup>) in aqueous dispersions was determined by the drying method. Following the work published by Lele et al.,<sup>37</sup> we considered that a particle is composed of 71 wt % of polymer and 29 wt % of bound water at 50 °C. From the hydrodynamic particle diameter,  $d_{50\text{ °C}}$ , measured by PCS at 50 °C, the particle concentration  $c_{\text{particles}}$  (expressed in cm<sup>−3</sup>) of the dispersions was estimated as follows:

$$c_{\text{particles}} = \frac{6c_{\text{polymer}}}{\pi(d_{50\text{ °C}})^3} \left( \frac{1}{\rho_{\text{polymer}}} + \frac{0.29}{0.71\rho_{\text{water}}} \right) \quad (1)$$

where  $\rho_{\text{polymer}} = 1.269 \text{ g·cm}^{-3}$ <sup>37</sup> and  $\rho_{\text{water}} = 0.988 \text{ g·cm}^{-3}$  are respectively the polymer and water densities.

We hypothesized that eq 1 was valid whatever the cross-linker density for two reasons. First, all microgels were synthesized at high temperature and consequently they were obtained in their collapsed state. As demonstrated by Varga et al.,<sup>38</sup> the amount of water incorporated in the shrunk microgels was almost constant in the explored BIS concentration range. As can be seen in Supporting Information Figure S2, the diameters obtained at low temperature were all close to 700 nm and only the sharpness of the transition was influenced by the cross-linking density. Second, the validity of this assumption was checked in refs 34 and 35. From Cryo-SEM imaging, we could determine the surface concentration,  $\Gamma$ , of the microgels with good accuracy. From the droplet size distribution of the emulsions, we derived the total oil/water surface area of the droplets,  $S_{\text{int}}$ . By using microgels labeled with fluorescent moieties, we observed that all the microgels were adsorbed at the air water interface (no free particles in the continuous phase). The product  $\Gamma S_{\text{int}}$  is thus providing the total number of microgels in the system. Within 5–10% precision, this product was equal to the total amount of microgels deduced from eq 1. The agreement between both values is indirectly validating our assumption.

**4. Emulsion Production.** Typical emulsion batches were composed of 14 g of aqueous phase containing microgels and 6 g of oil (mainly hexadecane and dodecane for evaluating the emulsion adhesion by optical observations and dodecane and heptane for cryo-SEM observations). This mixture was then stirred with an Ultra-Turrax T25 mixer, at constant speed (9500 rpm) for 30 s. Considering the rotor and gap dimensions, the shear rate corresponding to the rotation speed (9500 rpm) was about  $18 \times 10^3 \text{ s}^{-1}$ . Unless otherwise specified, the emulsification was carried out at 25 °C. We checked that stirring under such conditions (low speed and short time) did not induce a temperature rise above the microgel's VPTT.

Emulsions were usually prepared by exploiting the limited coalescence process.<sup>34,39–44</sup> The systems were emulsified with low amounts of particles so that the newly created droplets were insufficiently protected by the particles. When the agitation was stopped, the droplets coalesced, thus reducing the total amount of oil–water interface. Since the particles are irreversibly adsorbed, the coalescence process stopped as soon as the oil–water interface was sufficiently covered and the resulting emulsions exhibited remarkably

narrow size distributions ( $P < 30\%$ , where  $P$  is the polydispersity index defined by eq 2 (see below)).<sup>39</sup> The final average drop diameter depended on the initial amount of particles and on their arrangement at the interface. In the present case, the drop diameter could be tuned between 95 and 500  $\mu\text{m}$  as the microgels concentration was varied between  $8.0 \times 10^{10}$  and  $1.5 \times 10^{10} \text{ cm}^{-3}$  (with respect to the oil phase) irrespective of the alkane chain length (heptane, dodecane, or hexadecane). For a more detailed description of the limited coalescence applied to these systems, the reader can refer to Supporting Information Figure S3 and ref 34. In some specific cases, a larger amount of microgels ( $12 \times 10^{10}$  microgels per cm<sup>3</sup>) was used, leading to more polydisperse emulsions.

**5. Optical Microscopy Observations.** The size distribution of the emulsions was estimated by direct imaging using an inverted optical microscope (Zeiss Axiovert X100) and a video camera. Images were recorded and the dimensions of about 50 droplets were measured, so that both the surface average diameter  $D$  and the polydispersity  $P$ , defined by eq 2, could be estimated.

$$D = \frac{\sum_i N_i D_i^3}{\sum_i N_i D_i^2} \quad P = \frac{1}{D_m} \frac{\sum_i N_i D_i^3 |D_m - D_i|}{\sum_i N_i D_i^3} \quad (2)$$

where  $N_i$  is the total number of droplets with diameter  $D_i$ .  $D_m$  is the median diameter, *i.e.* the diameter for which the cumulative undersized volume fraction is equal to 50%.

**6. Cryo-SEM Observations.** Cryo-SEM observations were carried out with a JEOL 6700FEG electron microscope equipped with liquid nitrogen cooled sample preparation and transfer units. A small amount of emulsion was first deposited on the aluminum specimen holder. The sample was frozen in the slushing station with boiling liquid nitrogen. The specimen was transferred under vacuum from the slushing station to the preparation chamber. The latter was held at  $-150\text{ °C}$  and  $10^{-5} \text{ Pa}$  and was equipped with a blade used to fracture the sample. Once fractured, the sample was coated with a layer of Au–Pd and was then inserted into the observation chamber equipped with a SEM stage cold module held at  $-150\text{ °C}$ . Dodecane was preferred to hexadecane for cryo-SEM observations because of its low melting temperature ( $-9.6\text{ °C}$ ), which avoided oil crystallization during the freezing step. Moreover, dodecane was amorphous in the solid state, so the droplet interfaces remained spherical and smooth. Heptane was also used when light sublimation of the specimen was required. In this case, after fracturing the sample, the temperature in the preparation chamber was raised to  $-95\text{ °C}$  during less than 5 min before decreasing again the temperature and then inserting the sample into the observation chamber.

## RESULTS AND DISCUSSION

**1. Emulsions Observation.** Several batches were prepared with various cross-linking densities (1.5, 2.5, 3.5, 5, and 10 mol % BIS). All the synthesized pNIPAM microgels had comparable hydrodynamic diameters,  $d_{25\text{ °C}} \approx 700 \text{ nm}$ , at room temperature, and as expected, the microgels shrank when heated above their volume phase transition temperature (VPTT =  $33\text{ °C}$ ),  $d_{T > \text{VPTT}} \approx 300 \text{ nm}$  (see Supporting Information Figure S2).<sup>34</sup> In all cases, oil-in-water emulsions were obtained using microgels as unique stabilizers.

Hexadecane-in-water emulsions were produced at variable microgel concentrations and cross-linking densities exploiting the limited coalescence process because of the irreversible microgel anchoring. In ref 34, it was shown that the adsorbed microgels adopted a flattened fried-egg-like structure (see also Supporting Information Figures S1 and S3).

To test the generality of the observations, in addition to alkanes, silicon oils, toluene, octanone, and bromocyclohexane were probed. The emulsions were highly flocculated, irrespective of the oil nature and microgel concentration. Once the emulsification was achieved, the emulsions were



stored at rest, and the large drops tended to form a dense cream at the top of the recipient because of the density difference between the oil and the aqueous phase. After a few minutes of settling, the cream became very firm, as revealed by Figure 1a:

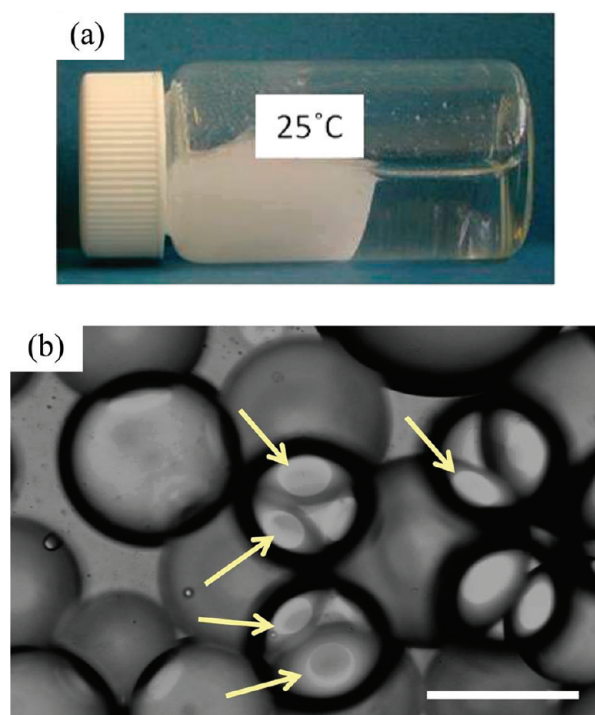


**Figure 1.** (a) Macroscopic image of a dodecane-in-water emulsion stabilized by 3.5 mol % BIS cross-linked microgels (number of microgels per unit volume of the oil phase:  $12.2 \times 10^{10} \mu\text{gels}\cdot\text{cm}^{-3}$ ): the cream forms a firm gel-like structure. (b) Optical microscopy image of a hexadecane-in-water emulsion stabilized by 1.5 mol % BIS cross-linked microgels ( $3.7 \times 10^{10} \mu\text{gels}\cdot\text{cm}^{-3}$  of hexadecane). The scale bar is 200  $\mu\text{m}$ . The arrows indicate the presence of adhesive films in between two drops.

when the vial was tipped over, the cream did not flow; instead it formed a rigid chunk that could hardly flow under its own weight. The firmness of the chunk was increasingly pronounced as the microgels cross-linking density increased.

**2. Film Adhesiveness. Adhesion Angle Measurements.** The aggregated state of the emulsions was confirmed by observations using an optical microscope. The emulsion drops were in close contact and were separated by flat films that appeared as white ellipses (see Figure 1b). Emulsion droplets exhibit such flat films when they experience pronounced attraction,<sup>1</sup> and a strong repulsion at short-range is then necessary to stabilize them against coalescence. Under such conditions, emulsion droplets form large adhesion angles as they adhere to one another. The adhesion is governed by the properties of the interfaces rather than by the nature of the phases in contact.

The first theoretical approaches of thin films and adhesion were mainly developed for thin soap films,<sup>1</sup> and we propose here to summarize some basic concepts about thin film thermodynamics. A thin liquid film can be modeled by two flat interfaces at a distance  $h$  apart from each other. The excess pressure in the film due to the interactions between the interfaces is defined as the disjoining pressure,  $\Pi_{\text{dis}}(h)$ .<sup>1</sup> For adhesive systems, the disjoining pressure is negative at a long

distance and it sharply rises at a shorter distance, ensuring stabilization against coalescence. Consequently, the interfaces spontaneously approach each other up to the equilibrium distance  $h_e$ . This distance is imposed by the sharp rise of the repulsion. The resulting work of adhesion,  $E_{\text{adh}}$ , is given by the following:

$$E_{\text{adh}} = E(h_e) = - \int_{\infty}^{h_e} \Pi_{\text{dis}}(h) dh \quad (3)$$

where  $E_{\text{adh}}$  is the free energy density of interaction. An important consequence resulting from the approach of the interfaces is that  $\gamma_f$ , the surface energy of the film, is lowered by the work of adhesion. When the interfaces are far apart,  $E(h)$  is equal to zero and  $\gamma_f$  is simply equal to  $2\gamma_{\text{int}}$ , where  $\gamma_{\text{int}}$  is the interfacial tension of a single interface. At equilibrium, the surface energy of the film is as follows:

$$\gamma_f = 2\gamma_{\text{int}} + E_{\text{adh}} \quad (4)$$

Since the tension of the film and the tension of two single isolated interfaces are different, an adhesion angle,  $\theta_{\text{adh}}$ , is expected at the junction between stuck and free interfaces, as schematized in Supporting Information Figure S4. The value of this adhesion angle is determined by the mechanical equilibrium that imposes:

$$\gamma_f = 2\gamma_{\text{int}} \cos(\theta_{\text{adh}}) \quad (5)$$

The adhesion angle is related to  $E_{\text{adh}}$  through:

$$E_{\text{adh}} = 2\gamma_{\text{int}}[1 - \cos(\theta_{\text{adh}})] \quad (6)$$

This relation, known as the Young–Dupré equation, shows that the energy density of adhesion can be obtained by determining both the adhesion angle and the surface tension of a single interface. As shown in Supporting Information Figure S4, the adhesion angle can be experimentally measured by looking at two adhesive droplets. However, a direct determination from edge views is rather difficult, especially if the adhesion angle is small. A more convenient way to estimate  $\theta_{\text{adh}}$  consists in measuring the radius of two adhesive droplets,  $R_1$  and  $R_2$ , and the radius of the adhesive film between the droplets,  $r$  (Supporting Information S3 Figure b), which are linked through the following equation:<sup>1</sup>

$$2\theta_{\text{adh}} = \text{Arcsin}\left(\frac{r}{R_1}\right) + \text{Arcsin}\left(\frac{r}{R_2}\right) \quad (7)$$

In the experimental images of Figure 1b, the adhesive films separating two drops appear as bright elongated ellipses (the arrows indicate some of them). Films can be distinguished because they do not reflect or transmit light as the surrounding oil–water interfaces do. The length  $r$  corresponds to the radius of the circle viewed from above or to the larger axis of the ellipse when observed in perspective (as sketched in Supporting Information Figure S4b).

Using this method, we measured the adhesion angle  $\theta_{\text{adh}}$  as a function of the microgel cross-linking density. The results for hexadecane-in-water emulsions are reported in Table 1. Each value was obtained from image analysis, after averaging the data over approximately 30 different adhesive films like those reported in Figure 1b. The same average values were obtained for dodecane-in-water emulsions (Table 2). We also checked that  $\theta_{\text{adh}}$  was independent of the average droplet radius, thus confirming that this parameter is governed by the properties of

**Table 1. Evolution of the Adhesion Angles, Estimated by Optical Microscopy, between Adhesive Hexadecane Droplets as a Function of the Microgels Cross-Linking Density and of the Drops Diameter**

microgels (BIS)	<i>D</i> (μm)	2θ <sub>adh</sub> (deg)
1.5 mol %	201	37 (±3)
	105	36 (±3)
2.5 mol %	214	44 (±5)
	119	46 (±4)
3.5 mol %	209	50 (±4)
	141	48 (±3)

**Table 2. Evolution of the Adhesion Angles, Estimated from Optical Microscopy and cryo-SEM Image Analysis, between Adhesive Dodecane Droplets as a Function of the Microgels Cross-Linking Density**

microgels (BIS)	2θ <sub>adh</sub> (deg) optical microscopy	2θ <sub>adh</sub> (deg) cryo-SEM
1.5 mol %	36 (±3)	40 (±5)
2.5 mol %	47 (±4)	45 (±5)
3.5 mol %	55 (±4)	54 (±5)

the interface only. Both sets of data reveal that the adhesion angle is an increasing function of the cross-linking density.

We also obtained cryo-SEM images like the one reported in Figure 2, which is a side view of a thin film sandwiched between

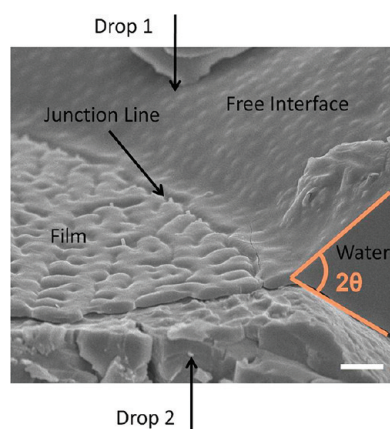


**Figure 2.** Cryo-SEM image of an adhesive film between two dodecane drops stabilized by 2.5 mol % BIS microgels. Example of adhesion angle determination at the junction between the thin film and the free interface. Scale bar is 2 μm.

two oil drops. After sample fracture, the frozen oil of the upper drop (drop 1) was detached, allowing direct visualization of the thin film and of the free interface. As studied in detail in ref 34, the adsorbed microgels on the free interface appear as lens-shaped bumps forming a hexagonal 2D array (see also Supporting Information Figure S1 and free interfaces in Figures 3, 4, 11, and 12). The structure of the film is more complex. A circular line can be discerned at the junction between the flat film and the free interface. From different side views of this type, it was possible to measure the adhesion angle.

In Table 2, we report the average angles resulting from cryo-SEM images for dodecane-in-water drops stabilized by microgels of variable cross-linking densities. For the sake of comparison, the values deduced from optical microscopy are indicated in the same table. Within experimental uncertainty,

there is no significant difference between the two sets of data. Moreover, the values are very close to those previously reported in Table 1 for hexadecane. This consolidates the conclusion that adhesion increases with the cross-linking density. Following eq 6, measuring the adhesion energy density  $E_{adh}$  would require determination of the oil/water surface tension. Obviously,  $\gamma_{int}$  depends on the coverage state of the microgels. As indicated above, emulsions undergo limited coalescence. To fabricate the emulsions, the mixture of oil and aqueous phase is stirred, and once the agitation is stopped, the droplets coalesce, thus reducing the interfacial area. Since the particles are irreversibly adsorbed, the interfacial density progressively increases.<sup>40</sup> In the final state, the adsorbed microgels are concentrated up to a point that there is no further coalescence between the droplets. The interfacial coverage resulting from stirring followed by limited coalescence may be different from the one resulting from spontaneous adsorption of microgels on an isolated interface. In conventional tensiometry measurements, the surface area remains constant over time and the samples are not submitted to agitation. Hence, surface tension measurements performed on single model interfaces are not necessarily reflecting the same interfacial coverage as in real emulsions. Consequently, we can only provide estimated values of the adhesion energy density.

The bare alkane–water surface tension at  $T = 25\text{ }^{\circ}\text{C}$  is close to  $50\text{ mN}\cdot\text{m}^{-1}$ <sup>45</sup> (it increases slightly with the alkane chain length, from  $50.7\text{ mN}\cdot\text{m}^{-1}$  for heptane to  $53.5\text{ mN}\cdot\text{m}^{-1}$  for hexadecane). Stimuli-sensitive emulsions stabilized by microgel particles consisting of poly(NIPAM-*co*-methacrylic acid) (pNIPAM-*co*-MAA) and being responsive to both pH and temperature were recently investigated with respect to the viscoelastic properties of the interfacial layer by Brugger et al.<sup>31</sup> The equilibrium interfacial tension at the heptane–water interface and at room temperature was equal to 13 and 16  $\text{mN}\cdot\text{m}^{-1}$  at pH 3 and pH 9, respectively. Monteux et al.<sup>46</sup> prepared poly(NiPAM-*co*-dimethylamino ethyl methacrylate) (pNIPAM-DMAEMA) microgels. The dodecane–water interfacial properties of the microgels were then investigated. At room temperature, the interfacial tension was close to 17  $\text{mN}\cdot\text{m}^{-1}$ . In the two previous references, although both the size and the composition of the microgels were different, the interfacial tensions were of the order of  $15\text{ mN}\cdot\text{m}^{-1}$ .

Considering the adhesion angles reported in Tables 1 and 2 (from 18 to  $27^{\circ}$ ) and a reasonable estimate of  $\gamma_{int}$  i.e.  $15\text{ mN}\cdot\text{m}^{-1}$ , we obtain  $E_{adh}$  values of the order of  $1.5\text{--}3\text{ mN}\cdot\text{m}^{-1}$ . Similar large values of the adhesion angles and of the adhesion energy were already reported in emulsions stabilized by anionic surfactants in the presence of highly concentrated electrolytes.<sup>47–49</sup> Poulin et al.<sup>49</sup> demonstrated that the liquid films separating the droplets were composed of two surfactant monolayers separated by a very thin ( $<1\text{ nm}$ ) aqueous layer. The adhesion was due to short-range attractive interactions between the surfactant layers. In the following section, we propose a detailed description of the film structure based on cryo-SEM imaging in order to assess the origin of the attraction between the emulsion drops.

**3. Film Observation.** Heptane or dodecane-in-water emulsions were prepared with microgels of variable cross-linking density. We then performed cryo-SEM experiments in order to resolve the structures of the particles. Our approach was based on observations of both edge and face views of the films, which provide complementary information. Finally, by provoking heptane and/or water sublimation of the frozen



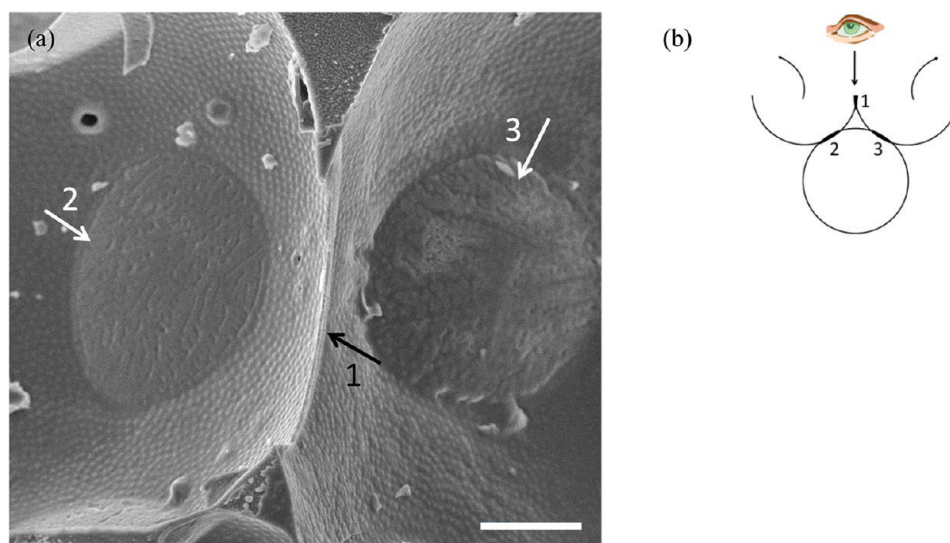


**Figure 3.** (a) Cryo-SEM image of contact zones between heptane drops stabilized by 2.5 mol % BIS microgels. Scale bar is 10  $\mu\text{m}$ . Three adhesive films can be observed in either edge view (indicated by the black arrow) or face view (white arrows) configuration. (b) Sketch of the three drops geometrical configuration.

specimens, the microgels were isolated and remnants of their initial state were kept, again providing useful structural information.

Figure 3 is a cryo-SEM image illustrating the different possible configurations in terms of film viewing. Figure 3b is schematic of the geometry of the sample. Three droplets are in contact, and after removal of the oil contained in the two upper drops, two adjacent cavities become apparent. A thin vertical film observed in the edge-view configuration is separating them (Figure 3a). The two almost circular patches indicated by the white arrows are face views of the films the two upper droplets have formed with the bottom one. The magnification of the image is sufficient to discern the hexagonal packing of the microgels on the free interfaces, but it is insufficient to resolve the structure of the films for both side and face view configurations.

In Figure 4, we report images of contact zones between drops stabilized by 2.5 mol % BIS microgels. Images a, b, and d were obtained with heptane, and image c corresponds to dodecane. The alkane chain length does not have any influence, since we observe the same interfacial structure for both oils. Figure 4 reveals that the film structure is very different from the one observed at free interfaces. The disk shaped films consist of a network of dendrites separated by constriction lines. The dendritic structure is more evident in the image of Figure 5, obtained at higher magnification. The dendrites are covered by microgels that remain lens-shaped and regularly located with almost the same spacing as in the hexagonal lattice on the free interfaces. The dendrites do not exhibit any preferential order and seem randomly distributed and oriented within the adhesive patches. The structure of the films varies with the cross-linking density, as evidenced in Figure 6. For the microgels with the lowest cross-linking densities (1.5 and 2.5 mol %), we only observed disordered dendritic networks like the ones already reported in Figures 4 and 5. However, for the most cross-linked microgels (3.5 and 5 mol %), the films exhibited higher levels of ordering. In Figure 6b and c, we can see discrete constriction points forming a very regular hexagonal lattice. Such ordered arrays coexisted with random

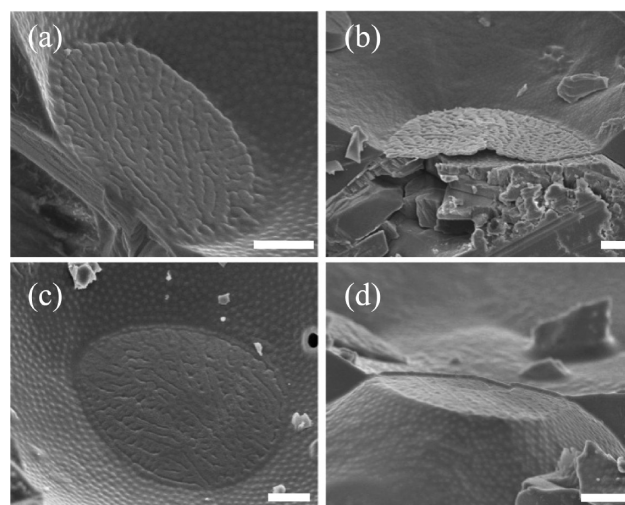


**Figure 4.** Cryo-SEM image of contact zones between drops stabilized by 2.5 mol % BIS microgels. The dispersed phase is heptane for parts a, b, and d and dodecane for part c. Scale bars are 5  $\mu\text{m}$ .

dendritic networks within the same emulsions and, in some cases, within the same adhesive film.

From the images of Figure 6b and c, we deduce that the average center-to-center distances between the constriction points in the hexagonal arrays are equal to 950 nm and to 750 nm for the 3.5 and 5 mol % BIS microgels, respectively. For the sake of comparison, the distance between the microgels adsorbed on the free interfaces is close to 1100 nm and is almost independent of the microgel composition.<sup>34</sup> Thus, the packing density in the thin films is not only higher than that in the free interfaces, but it also increases with the cross-linking degree.

In Figure 7 we propose two cryo-SEM edge views of adhesive films between dodecane drops stabilized by 2.5 mol % BIS microgels. The films are made of swollen cells of variable lengths but almost constant thickness. Owing to the observation angle, it can be stated that the cells are cuts of the dendrites observed in the side views. The thinner parts of

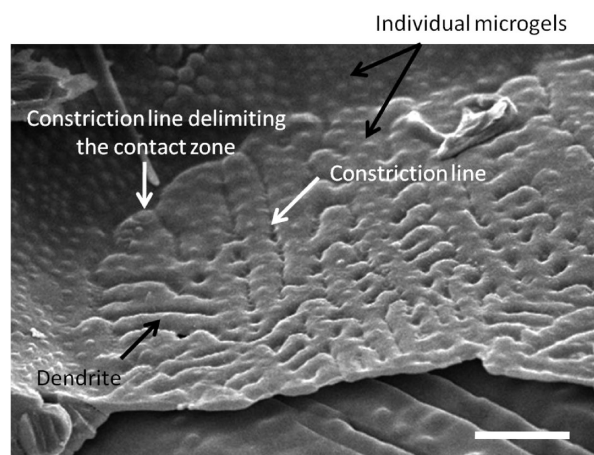


**Figure 5.** Cryo-SEM image of an adhesive film between two dodecane drops stabilized by 3.5 mol % BIS microgels. Scale bar is 5  $\mu\text{m}$ . The contact zone topology is complex and comprises individual microgels, dendrites, and constriction lines.

the films correspond to the above-mentioned constriction lines. A proper quantification of the average film thickness and of the density of constrictions as a function of the microgels cross-linking density would require a statistical analysis based on a large number of views. Unfortunately, images like that reported in Figure 7 were rather scarce because of the low probability for obtaining edge views of films. However, from the obtained images, we can conclude that the average cell thickness is varying between 500 and 700 nm and is in all cases lower than the hydrodynamic diameter of the non-deformed microgels at 25  $^{\circ}\text{C}$ . Some edge views of the hexagonal arrays of constrictions (3.5 and 5 mol % BIS) were obtained, and their thickness was even lower, between 250 and 500 nm.

Figure 8 (see also Supporting Information Figure S5) is an edge view of adhesive films between heptane drops stabilized by 2.5 mol % BIS microgels. After light sublimation, the polymer membrane, surrounding the cells, was highlighted (see Supporting Information Figure S5a). Then, sublimation was prolonged until almost complete evaporation of heptane and water was achieved, thus revealing the polymeric scaffold. The deswollen structure undergoes partial shape relaxation during the evaporation process, and the final structure is made of two parallel polymeric layers and orthogonal “bridges” in between them. Figure 8 is an example of the final structure resulting from full sublimation of the two immiscible phases, again exhibiting the “open” structure with cavities sandwiched in between two polymer layers and with orthogonal polymeric

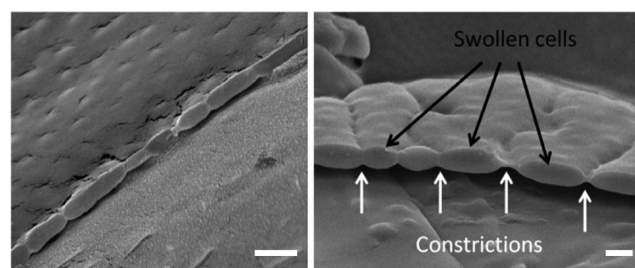


**Figure 7.** Cryo-SEM edge views of adhesive films between dodecane drops stabilized by 2.5 mol % BIS microgels. Scale bars are 1  $\mu\text{m}$ . Films are made of swollen cells separated by constriction lines.

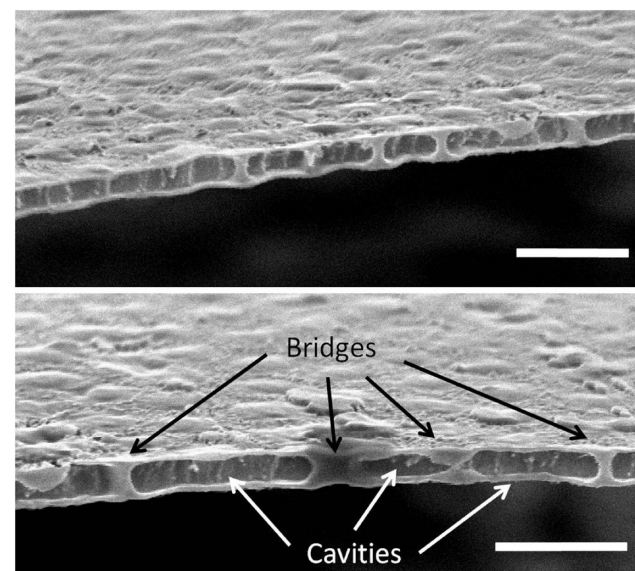


**Figure 8.** Edge views of fully dehydrated films between heptane drops stabilized by 2.5 mol % BIS microgels. Scale bars are 1  $\mu\text{m}$ .

bridges. The parallel layers are remnants of the monolayers formed by the microgels adsorbed on a single interface, whereas the bridges correspond to microgels that were simultaneously adsorbed on the two interfaces.

The same type of sublimation experiment was carried out starting with thin films made of a hexagonal array of constrictions (5 mol % BIS) (see Supporting Information Figure S6; the figure is a face view of the final state). The heptane and the water phases located below the film were removed, and in the end, a single thin monolayer remained in between the upper and bottom empty spaces. Only the central cores of the microgels are easily distinguishable. They are

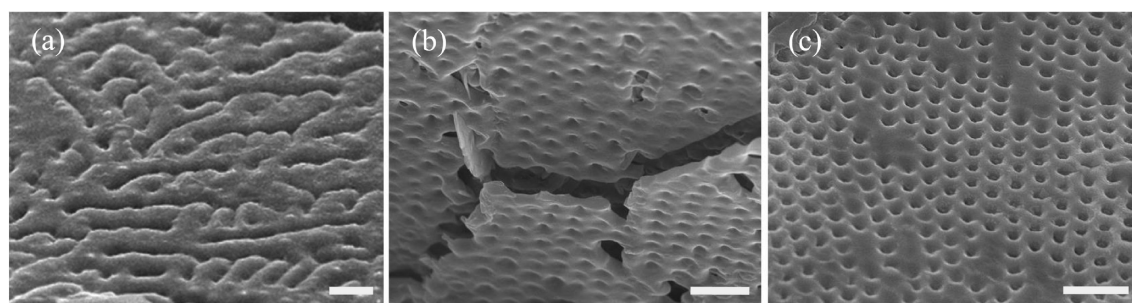


**Figure 6.** Structure of contact zones between dodecane drops stabilized by (a and b) 3.5 mol % and (c) 5 mol % BIS microgels. Scale bars are 2  $\mu\text{m}$ . The films exhibit dendritic (a) or hexagonal patterns (b and c).



surrounded by a very thin and hardly visible membrane formed by the overlapping of the (dehydrated) peripheral shells. This membrane ensures the interconnection of the microgels as well as their arrangement within the same plane (see also Supporting Information Figure S7).

**4. Discussion on the Film Structure.** From the previous analysis, we can propose a description of the thin adhesive film separating the droplets and of its evolution with the cross-linking density, as sketched in Figure 9. When the microgels are

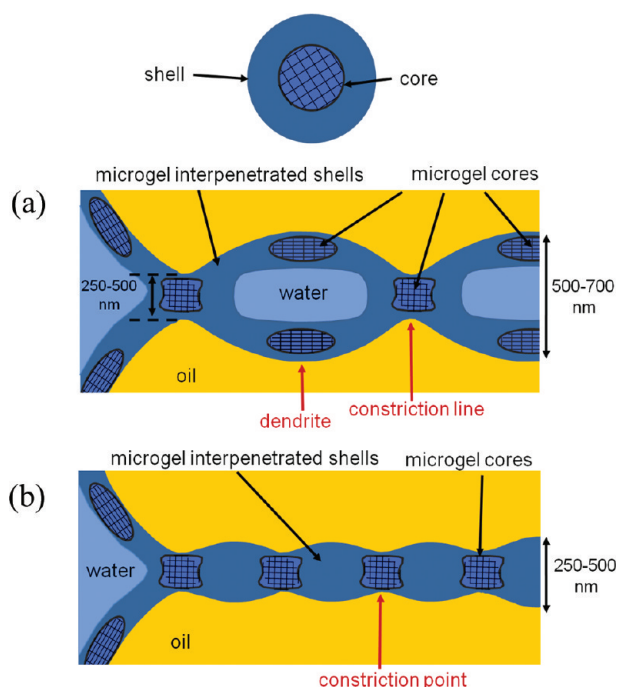


**Figure 9.** Sketches of the structures adopted by the films: (a) When the microgels are weakly cross-linked, some of them cover one interface only and some others bridge the two interfaces of the film. (b) For higher cross-linking densities (3.5 and 5 mol % BIS), most of the microgels bridge the two interfaces and form a hexagonal array of constriction points. For the sake of simplicity, only the cores of the microgels are represented whereas the shell is figured by a continuous dark blue zone.

weakly cross-linked, the density of bridging is rather low. The film can thus be seen as a bilayer with only a fraction of the microgels bridging the interfaces. These latter are not randomly distributed in the film, but instead they are positioned along constriction lines. As the cross-linking density increases, the probability for polymer bridging is enhanced and some films are single monolayers made of a hexagonal array of constrictions, reflecting the ordered packing of the microgels. Concomitantly, the packing density of the microgels in the films increases with the cross-linking degree. The undulated shape of the interface circumvallating the constriction points (Figure 6b and c) suggests that the film is thinner at the level of the cores and thicker at the level of the shells. It is likely that the microgels are compressed under the effect of attractive capillary interactions at a point that the peripheral overlapped shells form thick rings surrounding the cores (Figure 9b). In the image reported as Supporting Information Figure S6, the film was dehydrated, resulting in shape relaxation of the microgels. Upon dehydration, the overlapped shells flatten and ultimately form a very thin polymeric membrane around the cores.

**5. Correlation between Microgel Cross-Linking Density, Film Structure, and Emulsion Stability.** On the free interfaces, the microgels adopt a “fried-egg-like” structure, with a protruding core and a flat shell made out of long ramified digitations, as evidenced in Supporting Information Figure S1. This peculiar morphology is a consequence of the uneven distribution of the cross-linker within the microgels and of the amphiphilic nature of the polymeric segments. In ref 34, we underlined the empirical link between emulsion stability and microgels deformability and we discussed the origin of that link in terms of lateral overlapping and interfacial elasticity. At low cross-linking density, the shells are easily interpenetrable and form a dense and elastic 2D interconnected network that efficiently protects the drops against coalescence. Conversely, at a high cross-linking density or in the collapsed state ( $T > VPTT$ ), microgels deformability is considerably reduced, which is detrimental to their spreading, their anchoring at the interface, and their lateral overlapping. Chain interpenetration becomes less favorable, likely resulting in a reduced interfacial elasticity that becomes insufficient to avoid film rupturing (coalescence), especially when the emulsions are slightly agitated. Such highly cross-linked microgels-stabilized emulsions are therefore very fragile and hardly handleable.

Interestingly, there is also a clear correlation between the film structure and the resistance of the emulsions to mechanical disturbances: the emulsions formulated with the most cross-linked microgels exhibit the largest bridging extent and the highest susceptibility to coalescence under gentle manual shaking. Some possible scenarios for film formation can be inferred from the previous cryo-SEM observations. Thin film formation implies that the droplets surfaces are stretched, which leads to the spontaneous formation of bridges as a final stage of film thinning. Bridging requires removal of adsorbed polymer from the near-contact region as the interfaces approach. During the film formation process, water is squeezed away from the film and the adsorbed microgels tend to be dragged toward the peripheral parts. The mobility of the adsorbed microgels on the droplet surfaces is then a key parameter, as chains can respond to film compression by moving sideways. At a low cross-linking density, the strong interfacial connectivity (overlapping) of the microgels actually reduces their mobility. In this limit, the interface is rigid and brittle: as the two interfaces approach, they are stretched and undergo cracking. This phenomenon is probably at the origin of the constriction lines observed in cryo-MEB images. Microgel coils can extend from one surface to the other and make molecular contacts on both sides. One surface then provides the missing polymer to the other along the fracture lines. At a high cross-linking density, interfacial spreading and lateral chain interpenetration becomes less favorable. The cohesiveness of the adsorbed layer may become insufficient to avoid fragmentation of the 2D interconnected network and massive squeezing away of the microgels. Experimentally, this implies that the bridging phenomenon is more likely to occur. The images of Figure 6b and c and Supporting Information Figure S6 reveal that the film may become one monolayer thick, which is consistent with a fully bridged configuration.

**6. Anchoring Energy of the Microgels.** Microgels act as sticky particles in the thin films. An estimate of the anchoring (adsorption) energy,  $E_{\text{anch}}$ , of individual microgels at the oil–water interface can be deduced from the adhesive energy density of the films,  $E_{\text{adh}}$ , and from geometric considerations. Indeed, each microgel bridging two interfaces can be



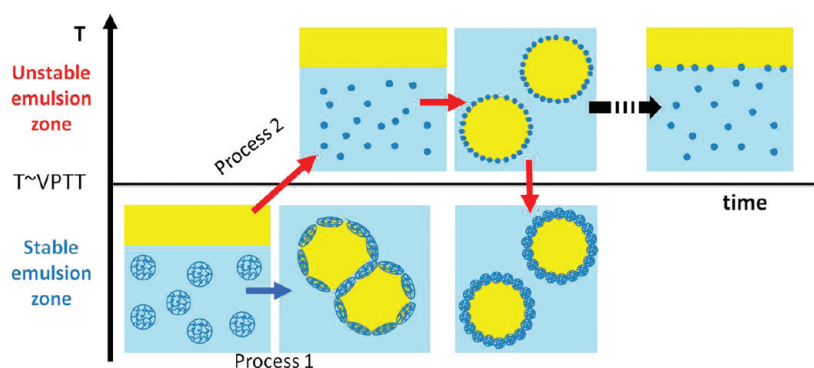


**Figure 10.** Scheme of the two emulsification pathways leading to distinct interfacial configurations. Emulsification can be performed at room temperature, leading to flocculated emulsions. Microgels are flattened and may bridge the interfaces, forming adhesive films between the drops (blue arrow). Emulsification at  $T > \text{VPTT}$  allows adsorption of microgels in their collapsed state. Upon quenching to  $T < \text{VPTT}$ , the volume expansion (swelling) produces high compaction of the monolayer (red arrows) that further protects the drops against bridging and coalescence. Cooling has to be fast enough to avoid phase separation that otherwise occurs within minutes.

considered as an independent sticking point whose contribution to the adhesion is equal to  $2E_{\text{anch}}$ . The total adhesion energy density can thus be expressed as:

$$E_{\text{adh}} = \frac{2NE_{\text{anch}}}{\pi r^2} \quad (8)$$

where  $N$  is the total number of bridging particles within a single adhesive patch of radius  $r$  (Supporting Information Figure S4):

$$N = \frac{f\pi r^2}{a_0} \quad (9)$$

In eq 9,  $a_0$  is the interfacial surface area occupied by one microgel and  $f$  is the fraction of microgels in the patches that bridge the two interfaces. By combining eqs 6, 8, and 9, we finally obtain:

$$E_{\text{anch}} = \frac{E_{\text{adh}}a_0}{2f} = \frac{a_0\gamma_{\text{int}}(1 - \cos \theta_{\text{adh}})}{f} \quad (10)$$

A reliable value of  $a_0$  can be obtained from the center-to-center distance ( $d_{\text{center-to-center}}$ ) of the microgels in the hexagonal arrays of constriction points (see section above); we obtain  $a_0 \approx 0.6 \mu\text{m}^2/\text{microgel}$ . Considering the adhesion angles reported in Tables 1 and 2,  $\gamma_{\text{int}} \approx 15 \text{ mN}\cdot\text{m}^{-1}$ , and  $f$  close to 1, the order of magnitude of the anchoring energy is  $E_{\text{anch}} \approx 8 \times 10^{-16} \text{ J}$ , that is  $(2 \times 10^5)kT$ , where  $kT$  is the thermal energy. This large value compared to the thermal energy reveals the irreversible anchoring of the soft particles. It is worth estimating the proportion of NIPAM segments contributing to the anchoring energy, considering the number of NIPAM segments per microgel, equal to  $3.5 \times 10^7$ , and the interaction energy,  $\delta$ , between one NIPAM monomer and the oil phase,  $\delta \approx 0.15kT$ .<sup>50,51</sup> The isopropyl side group carried by each monomer confers a small degree of hydrophobic character and is responsible for the surface activity of the microgels.<sup>50,51</sup> Hence, approximately  $5 \times 10^5$  segments in each microgel contribute to the anchoring of the particles at the oil–water interface, which corresponds to approximately 3% of the total number of NIPAM segments. This result is not surprising considering that only the peripheral parts of the microgels can actually interact with the oil phase.

The anchoring energy obtained in the previous paragraph has to be considered as an order of magnitude. It confirms that the microgels are irreversibly adsorbed at room temperature. This

is the first estimation of an anchoring energy of soft particles. It is now interesting to compare it with the anchoring energy of a solid (non-deformable) particle at an oil–water interface, which is given by the following equation:

$$E_{\text{anch,solid}} = \pi\gamma_0\left(\frac{d}{2}\right)^2 [1 \pm \cos(\theta_{\text{anch}})]^2 \quad (11)$$

where  $d$  is the particle diameter,  $\gamma_0$  is the bare oil–water interfacial tension, and  $\theta_{\text{anch}}$  is the 3-phase contact angle, defined as the angle between the particle tangent at contact and the interface, through the water phase.<sup>4</sup> Considering hydrophilic solid particles with the same diameter as our microgels in the expanded state ( $d = 700 \text{ nm}$ ), adsorbed at an alkane–water interface ( $\gamma_0 \approx 50 \text{ mN}\cdot\text{m}^{-1}$ ), the same anchoring energy would be reached for a  $\theta_{\text{anch}}$  value close to  $37^\circ$ . In the presence of soft particles, the concept of the 3-phase contact angle is obviously not relevant anymore because of their deformation. Like solid particles, microgels are embedded in both phases, but their immersion (protrusion) length is lower because of their flattened structure. Their deformation results from a competition between the intrinsic hydrophobicity of the NIPAM segments which tends to favor the spreading of the microgels at the interface in order to increment the number of “hydrophobic” anchoring points and the elastic resistance of the microgel particles controlled by their internal cross-linking density. The adsorption thermodynamics of soft particles is thus more complex than that of solid ones, although the same orders of magnitude of the anchoring energies can be achieved.

**7. Control of the Flocculated State through a Thermal Treatment.** The stability and flocculation states are determined by the ability of the monolayers to withstand stresses that tend to deform/stretch the interfaces during film compression. To enhance emulsion stability and avoid bridging flocculation, both the interfacial concentration of the microgels and their connectivity must be as high as possible. On the one hand, the connectivity is determined by the overlapping of the peripheral shells and is facilitated by the reduction of surface area occurring during the limited coalescence process. On the other hand, the interfacial concentration of microgels depends on the particle size during adsorption. In the remainder, we propose a method allowing optimization of these two parameters, *i.e.* compaction and overlapping of the microgels, ultimately leading to a significant reduction of adhesiveness and enhancement of emulsion resistance to mechanical stresses.

In Figure 10, we represent two possible emulsification pathways leading to very different interfacial configurations. In the first one (process 1), emulsification is carried out at room temperature and the resulting emulsions are strongly flocculated. This process was the one adopted up to now. The second process exploits the fact that, above the VPTT, microgels undergo a transition from the expanded (swollen) to the collapsed state. In this latter state, microgels are poorly efficient stabilizers, although they remain surface-active.<sup>30,31,45</sup> The mixture of oil and water was emulsified at  $T > \text{VPTT}$  and was then immediately quenched in an ice bath to  $T < \text{VPTT}$ . The cryo-SEM image of Figure 11 reveals the characteristic

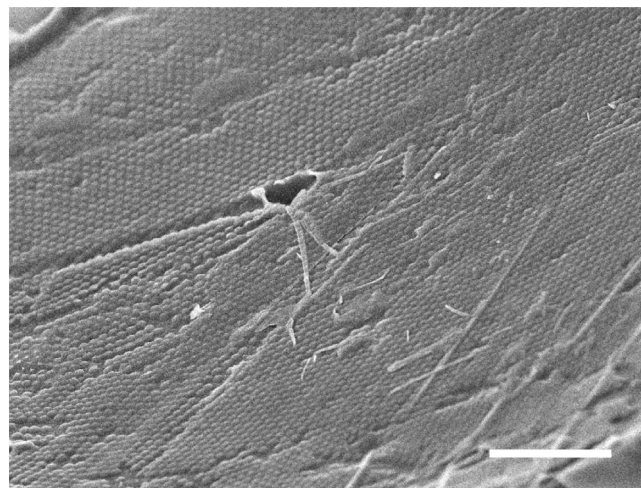


**Figure 11.** Cryo-SEM image obtained after cooling of a free interface in a dodecane-in-water emulsion stabilized by 3.5 mol % BIS microgels ( $12.2 \times 10^{10} \mu\text{gels}\cdot\text{cm}^{-3}$ ). Emulsification temperature = 41 °C. Scale bar is 5  $\mu\text{m}$ . The whole interface is covered by a hexagonally close-packed monolayer of compressed microgels.

final state (after quenching) of a free droplet interface. The system was stabilized by 3.5 mol % BIS microgels, and the emulsification was performed at 41 °C. We can clearly distinguish the hexagonally packed monolayer of microgels. The center-to-center distance, 475 nm, is significantly smaller than that in systems emulsified at room temperature, 1130 nm,<sup>34</sup> reflecting a much higher packing density. It is worth noting that this value is also much smaller than the hydrodynamic diameter of the initial microgels in aqueous solution (702 nm at 25 °C). The images of Figure 12 obtained after cooling at room temperature confirm that the average packing density increases as the emulsification temperature is raised from 25 to 41 °C. At the VPTT or just above, small clusters (short-range order) of hexagonally packed particles are formed and coexist with zones of lower density. The lateral extension of the clusters increases with the temperature until the hexagonal dense network becomes almost continuous (long-range order).

At  $T > \text{VPTT}$ , coalescence reduces the interfacial area and forces the almost non deformable spherical particles adsorbed at the interface to adopt dense hexagonal packing. Since the particles exhibit low lateral overlapping capacity in the collapsed state, the monolayer is fragile. It can be easily disrupted upon stretching, and the droplets are prone to coalescence. Under such conditions, coalescence-driven phase separation occurs within minutes. Most of the microgels leave the interface, as suggested by the turbidity appearing in the aqueous phase. As

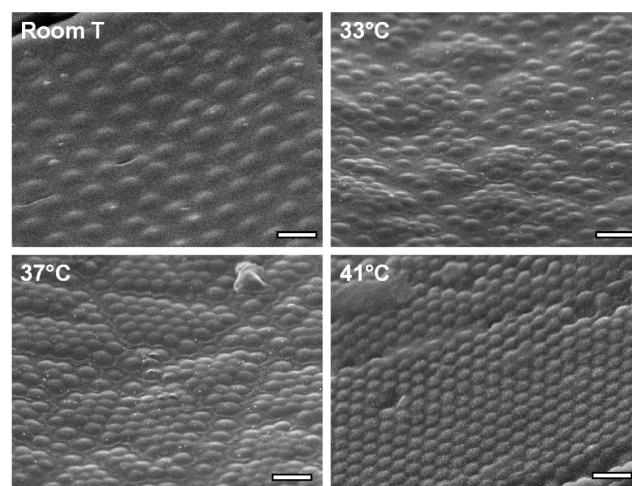


**Figure 12.** Cryo-SEM images obtained after cooling of free interfaces in dodecane-in-water emulsions stabilized by 3.5 mol % BIS microgels ( $12.2 \times 10^{10} \mu\text{gels}\cdot\text{cm}^{-3}$ ) as a function of the emulsification temperature. Scale bars are 1  $\mu\text{m}$ .

the emulsion droplets coalesce, the surface pressure of the monolayer becomes large enough to squeeze the microgels away from the interface. Indeed, it is likely that the anchoring energy is considerably reduced compared to the value that was previously calculated at 25 °C. In the collapsed state, the adsorbed microgels are less deformed than at 25 °C and the number of anchoring points per microgel is certainly reduced.

Hence, once the agitation is stopped, the sample has to be rapidly quenched to room temperature in order to restore the expanded state of the microgels (the transition being reversible) and to enhance their anchoring to the interface. During the swelling process (quenching to  $T < \text{VPTT}$ ), the high packing density is maintained. Because of the short center-to-center distance, the particles cannot expand laterally. However, they may expand along the normal to the interface and the monolayer thickness is thus expected to increase. In addition, monolayers are somehow laterally “fused” or “sintered” once the expanded state is recovered as the shells overlap. As a consequence, the resulting emulsions are remarkably stable against coalescence at room temperature, especially those fabricated at 41 °C.

In Figure 13, we report optical microscopy images of dodecane-in-water emulsions stabilized by 3.5 mol % BIS microgels, obtained at different emulsification temperatures from 25 to 41 °C (and immediately quenched), corresponding to Figure 12. They all were fabricated at the same oil volume fraction and with the same microgels concentration per unit volume of the oil phase, *i.e.*  $12.2 \times 10^{10} \mu\text{gels}\cdot\text{cm}^{-3}$ . The final average drop size increases with temperature (equivalently, the surface area of the droplets decreases), which is reflecting the evolution of the packing density of the microgels (the coverage capacity decreases). It should also be underlined that a fraction of the microgels remained unadsorbed when the emulsification was carried out above the VPTT. Indeed, the subnatant aqueous phase remained slightly turbid because of the presence of residual microgels. More interestingly, the large adhesive patches and adhesion angles previously observed by cryo-SEM and optical microscopy observations were no longer visible in the emulsions obtained following process 2 (Figure 13). The resulting emulsions were only slightly flocculated. This was confirmed by the spectacular evolution of the flow properties.



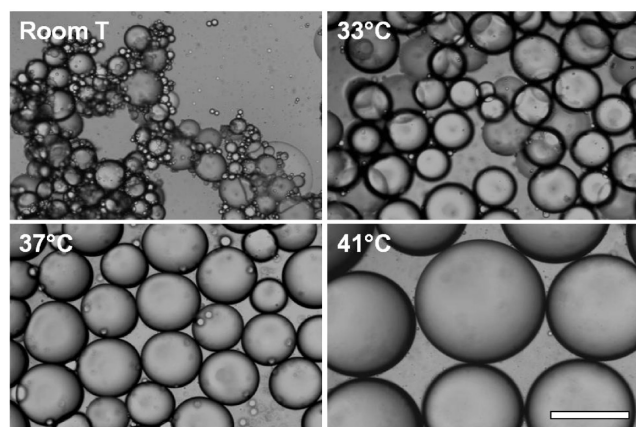


**Figure 13.** Optical microscopy images at room temperature of dodecane-in-water emulsions stabilized by 3.5 mol % BIS microgels ( $12.2 \times 10^{10} \mu\text{gels}\cdot\text{cm}^{-3}$ ) as a function of the emulsification temperature. Scale bar is 200  $\mu\text{m}$ . The drop size increases with the temperature, and adhesive films are no longer visible (as in Figure 1) when the emulsification is performed at  $T > \text{VPTT}$ .

Even after a storage period of several weeks, the creamed layers remained fluid, unlike the cases of the emulsions obtained through process 1. The difference in behavior is obvious by comparing Figure 1a and Figure 14. The same experiments

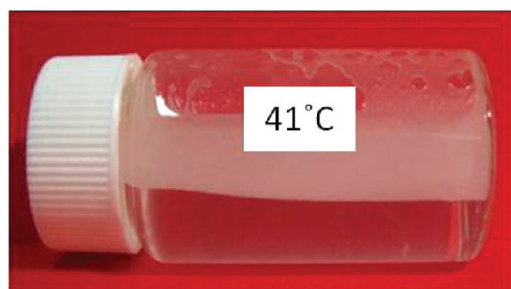


**Figure 14.** Macroscopic image (taken at room temperature) of a dodecane-in-water emulsion stabilized by 3.5 mol % BIS cross-linked microgels (number of microgels per unit volume of the oil phase:  $12.2 \times 10^{10} \mu\text{gels}\cdot\text{cm}^{-3}$ ) emulsified at 41  $^{\circ}\text{C}$  and quenched at room temperature. The cream remains fluid and flows under its own weight when the vial is tipped over.

were performed with 5 and 10 mol % BIS microgels, and the evolution was spectacular in terms of stability under flow. The systems directly emulsified at 25  $^{\circ}\text{C}$  were unstable under gentle manual shaking, whereas the systems emulsified at 41  $^{\circ}\text{C}$  could withstand strong mechanical disturbances without being destroyed.

Temperatures higher than 41  $^{\circ}\text{C}$  were probed, but it turned out that the cooling step was too long, so that the emulsions were partially destabilized: an oil layer appeared at the top of the recipient. As the temperature increases, a denser interfacial packing of the microgels can be achieved but the emulsions remain exposed to the instability region ( $T > \text{VTPP}$ ) for a longer period of time during the cooling step. A compromise has thus to be found. Within the experimental conditions that were adopted here, the optimal emulsification temperature for obtaining fluid, non flocculated, and highly stable emulsions was around 40  $^{\circ}\text{C}$ .

Emulsions prepared at  $T > \text{VPTT}$  and immediately quenched at room temperature remained temperature-sensitive. Indeed,

when heated above the VPTT, the emulsions underwent phase separation within a few minutes, exactly like those prepared at room temperature following path 1 sketched in Figure 10.

## CONCLUSION

In this paper, we investigated the impact of microgels cross-linking density on the adhesiveness of oil-in-water emulsions. We provided experimental evidence that the drop adhesion is due to bridging phenomena. We found a clear correlation between the particle deformability, the structure of the adhesive film, and the adhesion angle. Microgels with the lowest cross-linking density provide the best resistance against coalescence and the lowest probability for bridging flocculation. At the opposite, highly cross-linked microgels are poorly efficient stabilizers and the droplets are strongly flocculated. On the whole, this study revealed the importance of two key parameters in controlling the emulsion properties: the lateral overlapping of the microgels and their coverage density. The relevance of these parameters to emulsion stability becomes clear when one considers the dynamics resulting when two droplets approach each other. The main process governing these dynamics is the drainage of the intervening thin film of fluid that resists coalescence and bridging. The mobility of the droplet interfaces decreases with increasing interfacial connectivity or surface density. As a result, the boundary condition influencing the velocity profile within the draining film evolves from one that is highly fluid (leading to high bridging density) to one that is significantly rigid, thus providing more resistance to flow (leading to mainly bilayer films). By exploiting the thermal sensitivity of the microgels, we could trigger these parameters and therefore vary the interfacial packing density. It is worth noting that we thus revealed a fundamental difference with respect to low molecular weight surfactants, for which the interfacial concentration is generally a thermodynamic state variable and not a path function. This strategy and the underlying concepts were successfully utilized to reduce or suppress film adhesiveness (aggregation) and to improve the stability under flow of the emulsions without losing the temperature sensitivity of the emulsions. Hopefully, our results will open new perspectives for the formulation of stimulus-responsive emulsions and, more generally, for better control of emulsion end-use properties.

## ASSOCIATED CONTENT

### Supporting Information

S1: Morphology of the microgels adsorbed at emulsion drop surfaces, S2: List of typical synthesized microgels and main characteristics, S3: Important features of limited coalescence, S4: Scheme explaining the method used to determine the adhesion angle  $\theta_{\text{adh}}$ , S5: Edge views of adhesive films between adjacent drops, S6: Face views of adhesive films between adjacent drops, S7: Cryo-SEM views of fully dehydrated films between heptane drops stabilized by 5 mol.% BIS microgels. This material is available free of charge via the Internet at <http://pubs.acs.org>.

## AUTHOR INFORMATION

### Corresponding Author

\*E-mail: [m.destribats@hull.ac.uk](mailto:m.destribats@hull.ac.uk); [schmitt@crpp-bordeaux.cnrs.fr](mailto:schmitt@crpp-bordeaux.cnrs.fr).

## Present Address

<sup>‡</sup>University of Hull, Surfactant and Colloid Group, Department of Chemistry, Hull HU6 7RX, U.K.

## REFERENCES

- (1) Leal-Calderon, F.; Schmitt, V.; Bibette, J. *Emulsion Science. Basic Principles*, 2nd version; Springer: 2007.
- (2) Ramsden, W. *Proc. R. Soc.* **1903**, 72, 156–164.
- (3) Pickering, S. U. *J. Chem. Soc., Trans.* **1907**, 91, 2001.
- (4) Binks, B. P. *Curr. Opin. Colloid Interface Sci.* **2002**, 7 (1–2), 21.
- (5) Leal-Calderon, F.; Schmitt, V. *Curr. Opin. Colloid Interface Sci.* **2008**, 13 (4), 217.
- (6) Pieranski, P. *Phys. Rev. Lett.* **1980**, 45, 569.
- (7) Aveyard, R.; Clint, J. H.; Nees, D.; Paunov, V. N. *Langmuir* **2000**, 16, 1969.
- (8) Horozov, T. S.; Aveyard, R.; Clint, J. H.; Binks, B. P. *Langmuir* **2003**, 19, 2822.
- (9) Horozov, T. S.; Aveyard, R.; Clint, J. H.; Neumann, B. *Langmuir* **2005**, 21, 2330.
- (10) Asekomhe, S. O.; Chiang, R.; Masliyah, J. H.; Elliott, J. A. W. *Ind. Eng. Chem. Res.* **2005**, 44, 1241.
- (11) Xu, H.; Melle, S.; Golemanov, K.; Fuller, G. *Langmuir* **2005**, 21, 10016.
- (12) Kralchevsky, P. A.; Denkov, N. D. *Curr. Opin. Colloid Interface Sci.* **2001**, 6, 383.
- (13) Vella, D.; Aussillous, P.; Mahadevan, L. *Europhys. Lett.* **2004**, 68, 212.
- (14) Zang, D. Ph.D. thesis, Paris Sud 11 University, 2009.
- (15) Zang, D.; Stocco, A.; Langevin, D.; Wei, B.; Binks, B. P. *Phys. Chem. Chem. Phys.* **2009**, 11, 9522.
- (16) Zang, D.; Rio, E.; Langevin, D.; Wei, B.; Binks, B. P. *Eur. Phys. J. E* **2010**, 31, 125.
- (17) Zang, D.; Rio, E.; Delon, G.; Langevin, D.; Wei, B.; Binks, B. P. *Mol. Phys.* **2011**, 109, 1057.
- (18) Arditty, S.; Schmitt, V.; Leal-Calderon, F. *Eur. Phys. J. B* **2005**, 44, 381.
- (19) Arditty, S. Ph.D. thesis, Bordeaux 1 University, 2004.
- (20) Boufarguine, M. Ph.D. thesis, Maine University, 2011.
- (21) Bécu, L.; Benyahia, L. *Langmuir* **2009**, 25, 6678.
- (22) Stancik, E. J.; Kouhkan, M.; Fuller, G. G. *Langmuir* **2004**, 20, 90.
- (23) Stancik, E. J.; Fuller, G. G. *Langmuir* **2004**, 20, 4805.
- (24) Horozov, T. S.; Binks, B. P. *Angew. Chem., Int. Ed.* **2006**, 45, 773.
- (25) Xu, H.; Lask, M.; Kirkwood, J.; Fuller, G. *Langmuir* **2007**, 23, 4837.
- (26) Ngai, T.; Behrens, S. H.; Auweter, H. *Chem. Commun.* **2005**, 331.
- (27) Ngai, T.; Auweter, H.; Behrens, S. H. *Macromolecules* **2006**, 39, 8171.
- (28) Fujii, S.; Read, E. S.; Binks, B. P.; Armes, S. P. *Adv. Mater.* **2005**, 17, 1014.
- (29) Fujii, S.; Armes, S. P.; Binks, B. P.; Murakami, R. *Langmuir* **2006**, 22, 6818.
- (30) Brugger, B.; Richtering, W. *Langmuir* **2008**, 24, 7769.
- (31) Brugger, B.; Rosen, B. A.; Richtering, W. *Langmuir* **2008**, 24, 12202.
- (32) Koh, A. Y. C.; Saunders, B. R. *Langmuir* **2005**, 21, 6734.
- (33) Tsuji, S.; Kawaguchi, H. *Langmuir* **2008**, 24, 3300.
- (34) Destribats, M.; Lapeyre, V.; Wolfs, M.; Sellier, E.; Leal-Calderon, F.; Ravaine, V.; Schmitt, V. *Soft Matter* **2011**, 7, 7689.
- (35) Destribats, M. Ph.D. thesis, Bordeaux 1 University, 2010.
- (36) Wu, X.; Pelton, R. H.; Hamielec, A. E.; Woods, D. R.; McPhee, W. *Colloid Polym. Sci.* **1994**, 272, 467.
- (37) Lele, A. K.; Hirve, M. M.; Badiger, M. V.; Mashelkar, R. A. *Macromolecules* **1997**, 30, 157.
- (38) Varga, I.; Gilányi, T.; Mészáros, R.; Filipcsei, G.; Zrínyi, M. *J. Phys. Chem. B* **2001**, 105, 9071.
- (39) Arditty, S.; Schmitt, V.; Giermanska-Kahn, J.; Leal-Calderon, F. *J. Colloid Interface Sci.* **2004**, 275 (2), 659.
- (40) Arditty, S.; Whitby, C. P.; Binks, B. P.; Schmitt, V.; Leal-Calderon, F. *Eur. Phys. J. E* **2003**, 11 (3), 273.
- (41) Whiteside, T. H.; Ross, D. S. *J. Colloid Interface Sci.* **1995**, 169, 48.
- (42) Gautier, F.; Destribats, M.; Perrier-Cornet, R.; Dechézelles, J. F.; Giermanska, J.; Héroguez, V.; Ravaine, S.; Leal-Calderon, F.; Schmitt, V. *Phys. Chem. Chem. Phys.* **2007**, 9 (48), 6455.
- (43) Horozov, T. S.; Binks, B. P. *Angew. Chem., Int. Ed.* **2006**, 45 (5), 773.
- (44) Destribats, M.; Lapeyre, V.; Sellier, E.; Leal-Calderon, F.; Schmitt, V.; Ravaine, V. *Langmuir* **2011**, 27, 14096.
- (45) Zeppieri, S.; Rodriguez, J.; Lopez de Ramos, A. L. *J. Chem. Eng. Data* **2001**, 46, 1086.
- (46) Monteux, C.; Marlière, C.; Paris, P.; Pantoustier, N.; Sanson, N.; Perrin, P. *Langmuir* **2010**, 26, 13839.
- (47) Aronson, M. P.; Princen, H. M. *Colloids Surf.* **1982**, 4, 173.
- (48) Princen, H. *Colloids Surf.* **1984**, 9, 47.
- (49) Poulin, P.; Bibette, J. *Phys. Rev. Lett.* **1997**, 79, 3290.
- (50) Bruno, J. Ph.D. thesis, University Paris 6, 2000.
- (51) Jean, B.; Lee, L. T.; Cabane, B. *Colloid Polym. Sci.* **2000**, 278, 764.